CONTRAST MEDIA & MOLECULAR IMAGING

Received: 22 May 2015, Revised: 9 October 2015, Accepted: 19 November 2015, Published online in Wiley Online Library: 11 January 2016

(wileyonlinelibrary.com) DOI: 10.1002/cmmi.1679

MRI monitoring of nanocarrier accumulation and release using Gadolinium-SPIO co-labelled thermosensitive liposomes

Cyril Lorenzato[a], Chris Oerlemans[a], Merel van Elk[b], Willie J. C. Geerts[c], Baudouin Denis de Senneville[a,d], Chrit Moonen[a] and Clemens Bos[a]*

Encapsulation of anticancer drugs in triggerable nanocarriers can beneficially modify pharmacokinetics and biodistribution of chemotherapeutic drugs, and consequently increase tumor drug concentration and efficacy, while reducing side effects. Thermosensitive liposomes release their contents triggered by hyperthermia, which can be, for example, precisely delivered using an MR Imaging-guided focused ultrasound procedure. In such a scenario, it is attractive to demonstrate the accumulation of liposomes before applying hyperthermia, as well as to document the release of liposome content using MRI. To address this need, thermosensitive liposomes were developed and characterized, which were doubly loaded by iron oxide nanoparticles and Gd-chelate, as opposed to loading with a single contrast agent. When intact, the transverse relaxivity of the liposomes is high allowing detection of carriers in tissue. After heating the longitudinal relaxivity steeply increases indicating release of the small molecular contents. By choosing the appropriate MR sequences, availability and release can be evaluated without interference of one contrast agent with the other. Copyright © 2016 John Wiley & Sons, Ltd.

Additional supporting information may be found in the online version of this article at the publisher's web site.

Keywords: magnetic resonance imaging (MRI); drug delivery systems (DDS); thermosensitive liposomes (TSL); relaxometry; High Intensity focused ultrasound (HIFU); magnetoliposomes

1. INTRODUCTION

Even though the pharmaceutical industry has been successful in discovering drugs for the treatment of a variety of cancer types, cancer still remains one of the principal causes of death in developed countries (1). Often, the efficacy of chemotherapeutics is limited due to inadequate delivery of drugs to the tumor target tissue and/or severe side effects. Due to their biocompatibility (2) and their capability of carrying and protecting molecules (3–8), liposome formulations have been developed to improve pharmacokinetic along with of the toxicity of conventional anti-cancer drugs. Doxorubicin loaded liposomes (Doxil®), for example, has shown less dose-limiting adverse effects such as cardiomyopathy and myelosuppression as compared to free doxorubicin (9). Moreover, liposomes can be rendered responsive to mild temperature elevation (e.g. 39–42 °C) based on their lipid composition, allowing triggered release of their content at the tumor site, using a mild hyperthermia (HT) procedure (10). Preclinically, the use of thermosensitive liposomes as drug carrier combined with mild HT has been demonstrated to allow for the enhanced drug targeting to a locally heated tumor (11–15), resulting in increased intratumoral drug concentrations up to six to 30-fold (13,16–19) over the free drug.

Nevertheless, controlling the release of the liposome content *in vivo* remains challenging. In such a treatment scenario, there is a need for visualizing the biodistribution of the carrier, since otherwise accumulation of the nanocarrier at the desired location can only be assumed, all the more so when tumor tissue perfusion is highly inhomogeneous. Additionally, there is the need to confirm drug release. MRI is an attractive technique for this purpose because it allows for both localizing the drug carriers (20) and monitoring the release of their content (16,21–23). Furthermore, MRI can be used for temperature measurements of the tissue, which allows guidance of the HT procedure, for instance high-intensity focused ultrasound (HIFU) (24–29), used to induce liposomal release.

* *Correspondence to: C. Bos, Sr. Scientist, Imaging Division, University Medical Center Utrecht, Room Q 0S.208, Q 00.118, Postbus 85500,3508 GA Utrecht, the Netherlands. E-mail: C.Bos@umcutrecht.nl*

a *C. Lorenzato, C. Oerlemans, B. Denis de Senneville, C. Moonen, C. Bos*
University Medical Center Utrecht, Department of Radiology, Imaging Division, Heidelberglaan 100, 3584 CX, Utrecht, The Netherlands

b *M. van Elk*
Department of Pharmaceutics, Utrecht Institute for Pharmaceutical Sciences, 3584 CG, Utrecht, The Netherlands

c *W. J. C. Geerts*
Biomolecular Imaging, Bijvoet Center, Utrecht University, Padualaan 8, 3584 CH, Utrecht, The Netherlands

d *B. Denis de Senneville*
Institut de Mathématiques de Bordeaux, UMR 5251 CNRS/Université de Bordeaux, F-33400, Talence, France

Abbreviations: *TSL, thermosensitive liposome; Gd, Gadolinium; Fe, Iron; HIFU, High Intensity Focused Ultrasound; DDS, drug delivery systems; Gd-TSM, Gadolinium-loaded thermosensitive magnetoliposomes; TSM, Thermosensitive Magnetoliposomes; ME-SPGR, multi-echo spoiled gradient-echo.*

Initially, carriers containing paramagnetic MRI contrast agents were proposed for monitoring drug release (10,18). It was shown that the MR signal enhancement on T_1-weighted images triggered by the release of paramagnetic contrast agents from thermosensitive liposomes can, *in vivo*, be quantitatively correlated with the local co-release of a drug (19,22,23). However, these nanocarrier formulations do not allow for monitoring the biodistribution of the liposomes. This is, on the other hand, more effectively achieved by using superparamagnetic contrast agents to label the thermosensitive liposomes, e.g. iron oxide nanoparticles. The nanoparticles induce a transverse relaxivity (R_2^*) increase that is present even if the nanoparticle is encapsulated and not in direct contact with water. In addition, it has been shown that the liposome formulation in (20) allows monitoring release due to a modest decrease of R_2^* effects induced by changes in microscopic iron oxide distribution after disintegration of the liposome. However, in view of the limited contrast in R_2^* based imaging upon release, it would be advantageous to separate the detection of distribution and release in independent MR parameters. Therefore encapsulating R_1-based and R_2^*-based MR contrast agents into one liposomal carrier should be beneficial for imaging biodistribution and release in a local drug delivery procedure.

In this study, we show that co-loading of a paramagnetic and a superparamagnetic MR contrast agent, affecting R_1 and R_2^* respectively, in thermosensitive liposomes, allows for both monitoring liposomal biodistribution, as well as liposomal release. Therefore, three thermosensitive liposome formulations, loaded either with a chelated gadolinium complex, citrated iron oxide nanoparticles or both were developed. The MR properties before and after heating of these dual MR contrast agent formulations were measured and compared. Finally, the utility of these formulations in an *ex vivo* renal vasculature system was investigated.

2. RESULTS AND DISCUSSION

2.1. Citrated iron oxide nanoparticle synthesis

The superparamagnetic component in our formulation was based on maghemite (γ-Fe_2O_3) nanoparticles, which were stable at pH ≈ 2–3. Next, citrated-USPIOs, were obtained by the surface adsorption of citric acid, effectively yielding maghemite particles stabilized by electrostatic repulsion at pH = 7.4. The resulting citrate coating led to the re-dispersion of the nanoparticles after substitution of the unadsorbed-citrate excess by the PBS solvent and the adjustment of the pH to 7.4. The citrate adsorption was further confirmed by the positive to negative switch of the surface charge as measured by the ζ-potential (see Table 1.) The maghemite nanocrystal size of the citrated-USPIO was assessed by TEM (Fig. 1) and the mean diameter was 8.0 ± 1.6 nm and found to be in agreement with other reports (30,31). The characterization results of the synthesized ferrofluid are summarized in Table 1.

2.2. Liposome characterization

Three temperature sensitive liposome formulations with identical lipid composition encapsulating either ProHance (Gd-TSL), citrated-USPIO (TSM) or both (Gd-TSM) were prepared. The final concentrations of phosphorus, gadolinium and iron of these systems as determined by ICP-OES are shown in Table 1. Regardless of the molecular cargo, these preparations showed a similar hydrodynamic radius (≈100 nm). All T*m* values were between 41.4 °C and 41.9 °C (Table 1.). Liposome sizes on Cryo-TEM images were found in agreement with the hydrodynamic radius measured with DLS. For the TSM as well as the Gd-TSM formulation, all citrated-USPIOs were entrapped in the TSLs (Fig. 2). Liposomes were mostly unilamellar and USPIO were hardly aggregated within the vesicles. Before heating, the mean number of USPIOs per liposome was 3.0 ± 0.5 and 2.5 ± 0.4 for the TSM and the Gd-TSM, respectively. After heating, no significant differences were found ($p > 0.05$), 2.7 ± 0.7 and 2.1 ± 0.3 for the TSM and the Gd-TSM, respectively. In addition, no USPIOs were found outside of the liposomes after the phase transition, further confirming that USPIOs remained in the internal aqueous phase for both the TSM and the Gd-TSM formulations.

During the preparation of the liposomes however, a small USPIO residue precipitated after passing the liposome solution through the PD-10 column. This was most likely related to the citrate retention within the columns, which led to the destabilization and thus the flocculation of the remaining non-entrapped USPIOs (see also supplementary material S1).

2.3. Liposomes MR contrast properties

Since the Gd-TSM are loaded with iron and Gd, and the other liposomes lack either iron or Gd, we will compare the relaxivities of the formulations based on the total amount of liposomes, see Fig. 3. We used the phosphorus concentration as a measure of liposome quantity, the more so, since based on the DLS data the hydrodynamic size of all three TSL formulations was found to be equivalent. Normalized to the phosphorus concentration, before release, Gd-TSL relaxivities r_1, r_2, and r_2^* were found to be 0.1 $mM.s^{-1}$, 1.6 $mM.s^{-1}$ and 3.8 $mM.s^{-1}$, respectively. For the two citrated-USPIO loaded liposomes, Gd-TSM and TSM, similarly low r_1 values,

Table 1. Overview of the nanoparticle characterizations

USPIO / Liposome	R_h[b] (nm)	PDI	ζ pot. (mV)	Tm (°C)	DSC peak max. (°C)	[P] (mM)	[Gd] (mM)	[Fe] (mM)
USPIO[a]	22	0.17	46.6 ± 0.3	NA	NA	NA	NA	1682 ± 95[c]
Citrated-USPIO	25	0.20	−38.8 ± 0.7	NA	NA	NA	NA	382 ± 28[c]
Gd-TSL	98	0.04	−1.4 ± 0.7	41.9	43.8	55.3 ± 1.4[d]	39.1 ± 0.4[d]	NA
TSM	104	0.07	−1.7 ± 1.2	41.6	43.0	58.4 ± 1.6[d]	NA	6.8 ± 0.3[d]
Gd-TSM	102	0.06	−0.5 ± 0.6	41.4	43.2	60.7 ± 1.1[d]	58.2 ± 0.2[d]	8.9 ± 0.3[d]

[a]Positively charged maghemite ferrofluid before coating.
[b]Hydrodynamic radius.
[c]Measured by colorimetry quantification.
[d]Mesured by IPC-OES.
NA = Not Applicable.

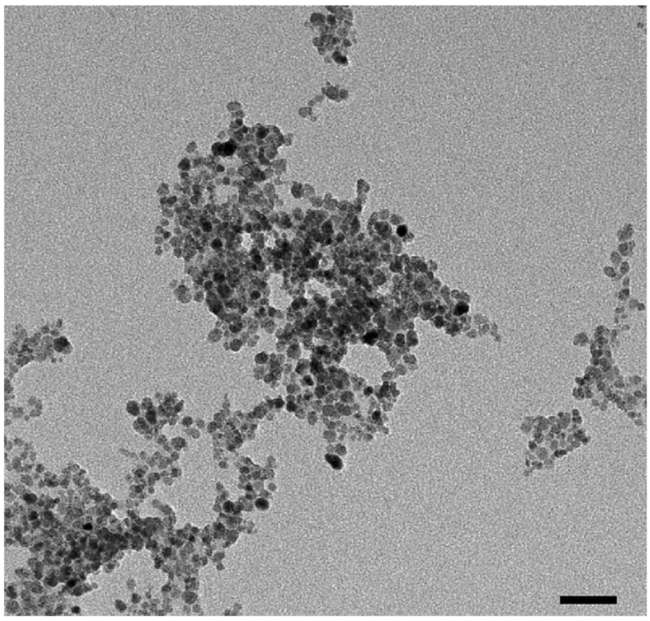

Figure 1. TEM images of the citrated iron oxide nanoparticles. Scale bars 50 nm.

$r_{1\ TSM} = 0.1\ mM.s^{-1}$ and the $r_{1\ Gd\text{-}TSM} = 0.3\ mM.s^{-1}$, were measured whereas high r_2 ($r_{2\ TSM} = 8.8\ mM.s^{-1}$, $r_{2\ Gd\text{-}TSM} = 13.2\ mM.s^{-1}$) and r_2^* ($r_{2\ TSM}^* = 11.9\ mM.s^{-1}$, $r_{2\ Gd\text{-}TSM}^* = 19.4\ mM.s^{-1}$) relaxivities were observed. After heating to 43 °C during 15 min, no significant variations were measured for free Citrated-USPIOs or TSM whereas r_1, r_2, and r_2^* of Gd-TSM were found to increase by a factor 14.0, 1.1 and 1.2 after release, Fig. 4. For Gd-TSL, finally, r_1, r_2, and r_2^* changed by a factor 27, 20 and 2.65, respectively.

We tested if these variations could be explained by the release of the chelated Gd-complex only. Thus, Gd-TSM relaxivities after release were estimated using Eq. 5 and found to be similar to the ones observed, $r_{1\ Gd\text{-}TSM}$ estimated $= 4.4\ mM.s^{-1}$, $r_{2\ Gd\text{-}TSM}$ estimated $= 15.5\ mM.s^{-1}$, $r_{2\ Gd\text{-}TSM}^* = 24.9\ mM.s^{-1}$. All measured relaxivities normalized to Gd or Fe concentration are summarized in Table 2.

The purpose of this study was to demonstrate that the encapsulation of both a paramagnetic and a superparamagnetic MR contrast agent in thermosensitive liposomes, provides a nanocarrier system with suitable switchable MR-properties for drug delivery monitoring by MRI. Whereas TSM allow for the detection of liposomes and Gd-TSL for characterizing their release, we combined these two properties into one formulation by the encapsulation of both a T_1 and a T_2^* contrast agent.

Different studies have shown that increasing the number of USPIOs inside the liposomes leads to an increase of both the r_2 and the r_2^* relaxivities (20,32,33). In our study, we observed that while the r_1 relaxivity of free citrated-USPIOs was reduced by a factor 5 after encapsulation in liposomes, both r_2 and r_2^* remained unchanged compared to free citrated-USPIOs (Table 2). The absence of r_2 and r_2^* differences is in agreement with

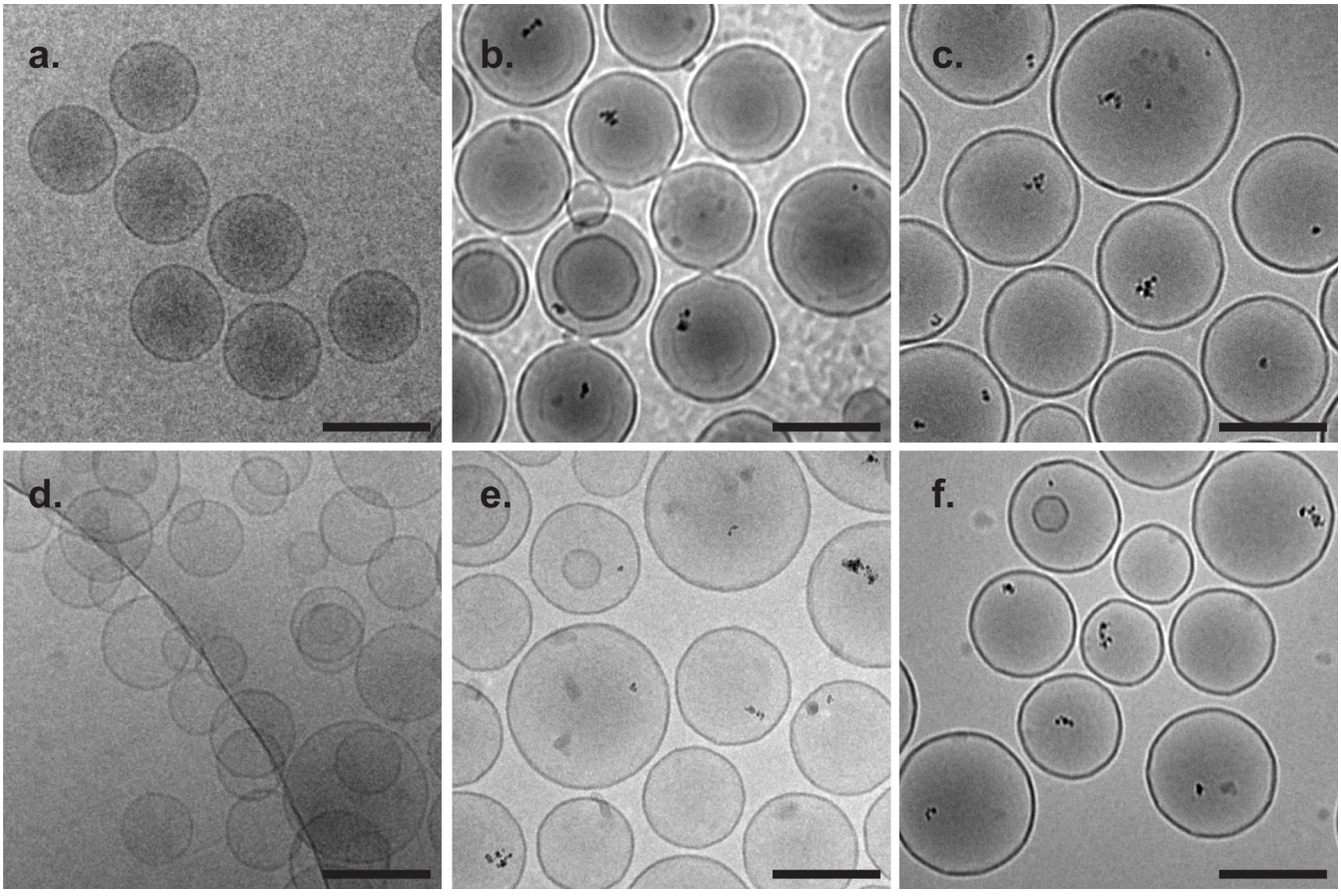

Figure 2. Cryo-TEM images of the three liposome formulations before (a-c) and after heating (d-f): Gd-TSL (a, d); Gd-TSM (b, e); TSM (c,f). Scale bars 200 nm.

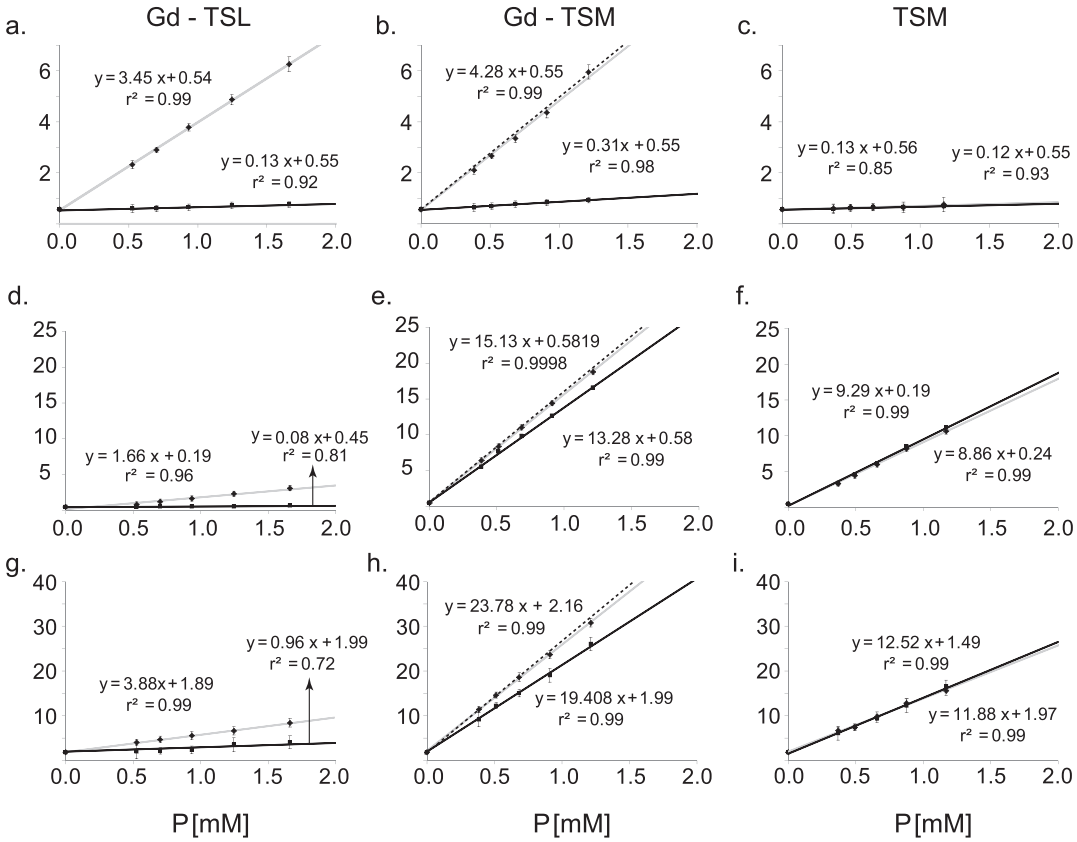

Figure 3. Relaxation rates R_1 (a-c), R_2 (d-f), R_2^* (g-h) vs. phosphorus concentration for comparison of r_1, r_2 and r_2^* relaxivities of the Gd-TSL, the Gd-TSM and the TSM formulations before (■) and after heating (♦) and the corresponding linear weighted fits over plots. Measurements were done at 1.5 T at room temperature.

previous studies, which showed that an increase of the transversal relaxivity is observed for formulations encapsulating at least 26 USPIOs per liposome of 100 nm in diameter (33). For to the USPIO-loaded liposomes, the TSM, neither the transversal nor the longitudinal relaxivity were found to be affected by the phase transition of the lipid bilayer triggered by heating. This suggests that the grain boundary permeabilization driven by the phase transition of the phospholipid bilayers (34) did not allow for USPIOs to escape from this liposome formulation. On Cryo-TEM, no USPIOs were found outside of the liposomes after the phase transition, further confirming that USPIOs remained in the internal aqueous phase for both the TSM and the Gd-TSM formulations. Conversely, the modest decrease of r_2^* observed in (20) was accompanied by release of USPIOs from the TSM, and subsequent dispersion of the particles after heating.

After heating, all Gd-TSL relaxivities were found to increase to the relaxivities measured for free chelated Gd while, before release, even a high solution concentration of encapsulated Gd (>1.5 mM) did not affect R_1. This indicates that the R_1 changes observed after heating were a consequence of the removal of the liposomal membrane that significantly limits the relaxivity of the paramagnetic contrast agent when encapsulated. Note, that all measurements were done at room temperature, to avoid confounding of these R_1 changes by an increase of the phosphobilayer permeability. In addition, the relaxation rates found for the Gd-TSM responded similarly to the heat induced release and could be closely predicted based on the Fe and Gd concentrations measured using ICP-OES (Fig. 3). This was in agreement with the scenario that the relaxivity variation of Gd-TSM is governed by the released chelated-Gd and the absence of USPIO release.

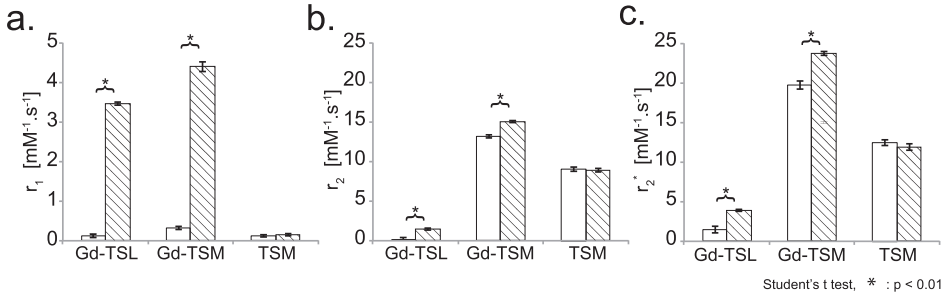

Figure 4. Relaxivities r1 (a), r2 (b) and $r2^*$ (c) with respect to the phosphorus concentration of Gd-TSL, Gd-TSM and TSM, respectively, before (solid bars) and after (hatched bars) heating. Measurements were done at 1.5 T at room temperature.

Table 2. Summary of the relaxivities before and after release

	[Gd]			[Fe]		
	r_1 ($mM.s^{-1}$)[a]	r_2 ($mM.s^{-1}$)[a]	r_2* ($mM.s^{-1}$)[a]	r_1 ($mM.s^{-1}$)[a]	r_2 ($mM.s^{-1}$)[a]	r_2*($mM.s^{-1}$)[a]
ProHance	4.5 | 4.7	4.9 | 4.8	5.5 | 5.2	NA	NA	NA
Citrated-USPIO	NA	NA	NA	5.3 | 5.2	79.5 | 80.1	94.9 | 96.8
Gd-TSL	0.2[c] | 4.9	0.15[c] | 4.9	2.8 | 5.5	NA	NA	NA
TSM	NA	NA	NA	1.0 | 1.3	79.8 | 79.7	107.5 | 99.9
Gd-TSM[b]	0.3[c] | 4.6	13.6 | 15.8	20.7 | 23.8	2.1 | 29.8	89.9 | 102.4	134.3| 160.9

[a]Before heating | After heating = 43 °C for 15 min. NA = Not Applicable.
[b]The relaxivities of the Gd-TSM resulted from both the presense of gadolinium and iron.
[c]5% < Standard deviation < 40%, for other values Standard deviation < 3%. Measurements were done at 1.5 T at room temperature.

2.4. MR-monitored HIFU heating

To demonstrate that Gd-TSM can be used to detect the availability of the carrier in a vasculature system and then to monitor the release process, a triggered release by localized HIFU treatments was performed on freshly resected kidneys that were collected from rabbits after they were terminated as part of another non-conflicting experimental protocol. Figure 5 shows the relaxation rate maps acquired prior to the injection of Gd-TSM, as well as the ΔR_1, ΔR_2 and ΔR_2^* maps after the liposome injection and the HIFU treatments. After liposome injection, no R_1 change was observed. Although only a small ΔR_2 located at the lobar and interlobar vessels was observed, ΔR_2^* values up to 100 s^{-1} were measured at the same location. 15 minutes after the first HIFU-triggered release the ΔR_2^* map was almost similar as prior to HIFU exposure, whereas changes in R_1 (≈1.4 s^{-1}) and R_2 (≈5 s^{-1}) were measured located in the heated region. The second HIFU heating, which was performed on the other side of the kidney, led to an equivalent ΔR_1 and ΔR_2 response, which was strongest near the vasculature system. T2-weighted magnitude images, which are sensitive to both R_1 and the R_2 changes, showed the presence of the liposomes in the veins by local hypointensities due to a signal dephasing effect (R_2) while the diffusion of the released Gd near the vasculature system led to localized hyperintensities surrounding the vessels.

In summary, Gd-TSM allowed for monitoring both the carrier availability and characterization of the release pattern as we have demonstrated in an *ex vivo* vasculature system, which was not possible using single label TSL (See supplementary data Fig. S2, S3). The R_1 and R_2 increase observed after the release triggered by the two HIFU heating procedures was, qualitatively, in accordance with the relaxivity variations measured *in vitro* before/after release. Previously, it has been shown that using thermosensitive liposomes co-encapsulating doxorubicin and manganese (19), or Gd-HPDO3A(Prohance) (23) as MR contrast agent allowed for quantifying the intratumoral deposition of the chemotherapeutic drug. Whereas the pharmacokinetic (PK) properties of the payload before release are governed by the nanocarrier, after release the PK properties of the released contrast agent and the released drug have to be comparable in order to achieve a 'chemo-dosimetry', based on imaging contrast changes. Hence, for each drug contrast-agent combination this correlation has to be validated, similar to what was done for manganese or [Gd(HPDO3A)(H2O)], and doxorubicin (23).

Still, with liposomes loaded with paramagnetic contrast agents, such as [Gd(HPDO3A)(H2O)], it was challenging to predict the distribution of the carrier, potentially leading to an incomplete tumor treatment for heterogeneous tumor morphology, e.g. due to the presence of a poorly vascularized core (35,36). In this study, we used a relatively weak iron concentration in order to obtain nanocarriers that can increase a typical soft tissue R_2^* (20 to 30 s^{-1}) by 20% after a 100-fold dilution of the systemic injected solution. Nevertheless, a strong R_2^* effect as a result of, e.g. local accumulation of Gd-TSM / iron into the tumor tissue, may also limit such an MR monitored drug delivery process. A too strong R_2^* increase will reduce the precision and/or the accuracy of MR temperature measurements (37–39) and thus the capability to guide the HT procedure with MRI. With respect to conventional PRF thermometry, based on a gradient echo sequence with an echo time of 20 to 30 ms, and assuming that a standard deviation of ± 0.5 °C is an acceptable upper limit for controlling the HT procedure, R_2^* of the order of 100 s^{-1} will represent an upper limit. In our *ex-vivo* kidney experiments, where MR thermometry was used to measure the temperature evolution, we therefore intentionally limited the iron and Gd dose injected. As an alternative, radiolabeling in combination with nuclear imaging techniques, e.g. single photon emission computed tomography (SPECT) or positron emission tomography (PET), are frequently used for quantitative *in vivo* biodistribution and pharmacokinetic studies (23,40,41). Being valued for their sensitivity, these imaging methods also have a limited influence of the environment on the radiolabel, thus allowing for accurate quantification of (drug-and carrier-associated) radiolabel accumulation. However, for the same reason, nuclear imaging prohibits discrimination of the state of the nanocarriers, and therefore to detect drug release (11), as we were able to demonstrate here using MRI.

In xenograft and murine tumor models it has been demonstrated that by using mild HT to release drugs from thermosensitive liposomes locally, can increase the drug concentration in the tumor area significantly (13,16–18) e.g. for doxorubicin loaded TSL, Viglianti *et al.* (19) observed an increase in tumor concentration of up to 30-fold over the free drug and five-fold over the total doxorubicin from a formulation similar to Doxil™, respectively. Also in rabbits, using a VX2 tumor model, Staruch *et al.* achieved a 26.7-fold increase of doxorubicin concentration in HT treated tumors vs. tumors not receiving HT (42). Besides serving as the trigger for release, hyperthermia can serve to increase the extravasation of carriers (11,12,14,15,18,37,43). Li *et al.*, for example have (14) demonstrated for three different tumor models that application of HT well before injection of the

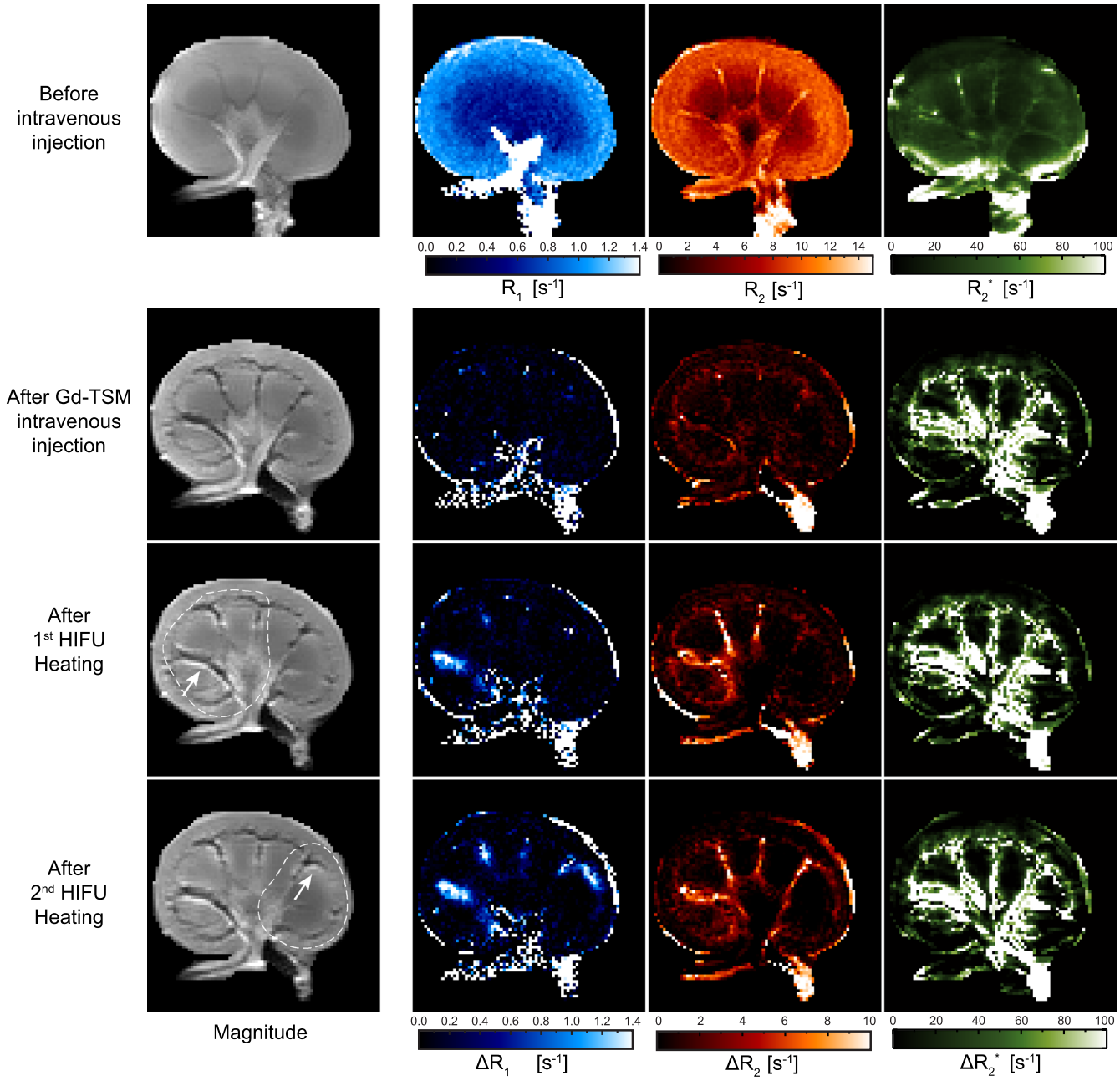

Figure 5. Relaxation rate maps obtained during the rabbit kidney treatment. Left side: T2 weighted magnitude images acquired at the different steps. Right side: Relaxation rate maps (R1, R2 and R2*) prior to any treatment followed by the corresponding variations measured after the Gd-TSM injection and the two consecutive HIFU treatments respectively. Measurements were done at 1.5 T at room temperature.

TSL, improved the distribution of the carriers in the tumor extracellular space. In several preclinical studies, in mice (13,16,18,22,26) and rat (44) models, it was demonstrated that the drug delivery procedure using TSL and HT effectively decreased tumor growth rate. Our results indicate that labeling the carrier using USPIOs should allow for demonstrating the availability of the carrier before the release step. This should be beneficial for preclinical experiments studying, for instance, the increase the of liposomes uptake of tumor mediated by a post mild HT treatment or active targeting drug delivery strategy (45,46) or even later, in clinical scenarios, to confirm the accumulation of the carrier before proceeding to the HT mediated release application.

We presented an MR imaging approach to detect availability and release of nanocarriers. However, for preclinical *in vivo* demonstration of this approach in drug delivery some additional challenges have to be met. Firstly, the physiologic stability of the presented formulation needs additional testing and, the feasibility of triple loading the liposomes with two contrast agents and a drug, would have to be studied.

3. CONCLUSIONS

This work demonstrated preparation and characterization of an MR observable thermosensitive liposome formulation co-loaded with a

paramagnetic and a superparamagnetic MR contrast agent, Gd-HP-DO3A and USPIO respectively. This concept should thus allow for MR monitoring of the drug delivery process, from the biodistribution of the carriers to the localized release of the contents.

4. EXPERIMENTAL

4.1. Materials

Iron(II) chloride, $FeCl_2$; Iron(III) chloride, $FeCl_3$; Hydrochloric acid, HCl (37%), Ammonium hydroxide, NH_4OH (28%), Nitric acid, HNO_3 (65%), Iron(III) nitrate, $Fe(NO_3)_3$; Citric acid; Hydroxylamine hydrochloride, $NH_2OH \cdot HCl$; 1,10 phenanthroline, Ethanol (96%) and Cholesterol were purchased from Sigma-Aldrich® (Chemie BV, Zwijndrecht, the Netherlands). DPPC, DSPC and DSPE-PEG_{2000} were purchased from Lipoid GmbH® (Cologne, Germany). ProHance® (Gadoteridol 0.5 M) was obtained from Bracco Imaging (Bracco Diagnostics Inc., NJ, Cranbury, USA). PD-10 columns were purchased from GE Healthcare (Little Chalfont, UK). Select Agar powder and Phosphate-Buffered Saline (PBS) were purchased from Invitrogen™ Life Technologies (Carlsbad, CA, USA).

4.2. Citrated ultrasmall superparamagnetic iron oxide nanoparticles synthesis

Citrated superparamagnetic maghemite particles (citrated-USPIO) were prepared based on a two-step procedure. First, the iron oxide nanoparticles were synthesized by co-precipitation of Fe^{II} and Fe^{III} chlorides (Fe^{II}/Fe^{III}, molar ratio 0.5) in alkaline conditions to obtain a maghemite (γ-Fe2O3) cationic ferrofluid as reported previously (30). An anionic ferrofluid, which is stable at pH 7.4, was then obtained by the electrostatic adsorption of negatively charged citrate molecules. For that purpose, a solution of $FeCl_2$ (dissolved in the presence of HCl) and $FeCl_3$ was prepared (Fe^{II} 33 mM / Fe^{III} 66 mM). Under strong stirring conditions, 30 mL of NH_4OH (8.6 M) was added rapidly to 370 mL of the Fe^{II}/Fe^{III} solution. A black anionic flocculate of nanoparticles was obtained and magnetically decanted in order to remove the supernatant. Subsequently, the adsorbed NH^{4+} ions were substituted with NO_3^- to obtain a cationic flocculate of magnetite in the presence of HNO_3 (20 mL, 2 M). After removal of the supernatant, core oxidation of the flocculate was achieved by the addition of 60 mL of Fe^{3+} ($Fe(NO_3)_3$, 0.33 M at 100 °C for 30 min) and another treatment with HNO_3 (20 mL, 2 M) at room temperature was performed. Next, the flocculate was washed three times with 200 mL acetone, and the nanoparticles were dispersed in demineralized water. Finally, the remaining acetone was completely removed by rotary evaporation under vacuum (Rotavapor R-210, BUCHI Laboratory Equipment, Zurich, Switzerland) at 40 °C. The citrate coating was obtained by addition of 10 mL USPIO dispersion to 30 mL citric acid (170 mM) leading to flocculation of the colloid. The flocculate was then washed rapidly with 40 mL demineralized water to remove the excess citrate and the citrated-USPIOs were recuperated in 40 mL PBS. Finally, the pH was adjusted to 7.4 by drop by drop addition of 0.1 M HCl leading to the re-dispersion of the citrated-USPIOs. The resulting ferrofluid was then filtered through 100 nm diameter pore filters and stored at ambient temperature.

4.3. Mohr's salt based colorimetric method

The iron content of the citrated-USPIO solution was determined using the 1,10-phenanthroline colorimetric method (47). First, 20 μL of concentrated hydrochloric acid and the solution was added to 40 μL of the USPIO dispersion and incubated for 1 h at room temperature to dissolve the USPIOs. Next, 100 μL of hydroxylamine hydrochloride (10%) was added, to reduce Fe^{III} to Fe^{II}, followed by the addition of 500 μL of 1,10 phenanthroline 3 mg/mL to form the orange-red complex of tris(1,10-phenanthroline) iron(II). Finally, the sample volumes were adjusted to 2 mL using ammonium acetate 500 mM pH 4 buffer, which was also used in the reagents' solutions. The absorbance of the samples was measured at 510 nm using a UV - vis spectrophotometer (Shimadzu UV/VIS 2450 spectrophotometer, Shimadzu Suzhou Instruments, Kyoto, Japan). The concentration of iron (II) was calculated using a calibration curve obtained using Mohr's salt solution ($(NH_4)_2Fe(SO_4)_2$) in HCl 0.01 M in a concentration range of 0.5–7.5 μg/mL.

4.4. Determination of ζ-potentials

To assess colloidal dispersion stability and to confirm the citrate coating, the ζ-potential was measured using a Nano Zetasizer (Z, Malvern, UK) at 25 °C. Both the positively charged USPIO and the citrated-USPIO were diluted 100 times in PBS (pH 7.4). Each sample was analyzed in triplicate.

4.5. Liposome preparation

Three different thermosensitive liposomes (TSL) were prepared using the thin-film hydration technique as described previously (48). The TSL formulation consisted of DPPC, DSPC, cholesterol and DSPE-PEG_{2000} in a molar ratio of 67:15:13:5 with a phospholipid concentration of 80 mM (49). The lipid mixture was obtained by dissolving lipids in 10 mL ethanol. After the lipids were completely dissolved, the solvent was evaporated to dryness by rotary evaporation under vacuum (Rotavapor R-210, BUCHI Laboratory Equipment, Zurich, Switzerland) and the resulting lipid film was further dried under a stream of N_2 during 24 hours. The first liposome formulation was hydrated with 250 mM of ProHance, the second formulation was hydrated with citrated-USPIO solution (50 mM iron content), the third formulation was hydrated with both 250 mM ProHance and citrated-USPIO solution (50 mM iron content), respectively. All three solutions used for lipid film hydration were first diluted in 10 mM HEPES-Buffered Saline (HBS), containing 135 mM NaCl, with a pH adjusted to 7.4. The resulting liposome dispersions were sized with sequential extrusion using a Lipex Extruder (Northern Lipids Inc., Vancouver, Canada) and polycarbonate membrane filters (Poretics Corporation, Livermore, CA, USA) with pore diameters of 600, 400 and 200 nm (two times each). Extra-liposomal ProHance, citrated-USPIO and the citrate molecules were substituted with PBS buffer using PD-10 columns (GE Healthcare, Little Chalfont, UK) for four consecutive times. The liposomal solutions were stored at 4 °C.

4.6. Dynamic light scattering measurements

The average hydrodynamic size and PDI of the liposome formulations and the (non-)citrated USPIOs were determined with dynamic light scattering (DLS) using a Malvern ALV CGS-3 system (Malvern Instruments Ltd., Worcestershire, UK). Intensity correlation functions were measured using a wavelength of 632.8 nm at a scattering angle of 90 °. Size and PDI determination was performed on liposome dispersions before and after the PD-10 extrusions.

4.7. Differential scanning calorimetry

For each liposome formulation, the phase transition temperatures (T_m) was determined with differential scanning calorimetry using a capillary cell microcalorimeter instrument (MicroCalVP-DSC, Northampton, MA, USA). The samples were heated with 2 °C min^{-1} from 25 °C to 55 °C, after an equilibration period of 10 min at 25 °C. The T_m values reported are the onset of the differential scanning calorimetry (DSC) peak. All measurements were performed in triplicate.

4.8. Transmission electron microscopy

Cryogenic transmission electron microscopy (cryo-TEM) was used to assess the morphology of the liposome preparations and to determine the localization of the citrated-USPIO within the liposomes before and after thermal treatment (15 min, 43 °C). Cryo samples were made by applying a liposome solution (2.5 μL, diluted at 1 mM of phosphorus concentration) onto a 200 mesh holey carbon Quantifoil grid (Quantifoil Micro Tools GmbH, Jena, Germany) and subsequently plunge frozen into liquid ethane 2.5 or liquid ethane 3.5 (Linde Gas, Schiedam, the Netherlands) using a Vitrobot II system (FEI, Eindhoven, the Netherlands). Cryo TEM studies were performed using a Tecnai 20 LaB6 transmission electron microscope (FEI, Eindhoven, the Netherlands) at 200 kV and a Gatan 626 single tilt cryo holder (Gatan, Munich, Germany). Cryo-TEM samples were maintained at temperatures below minus 167 °C. Images were recorded using a 4 K square pixel Eagle CCD camera (FEI, Eindhoven, the Netherlands). The Cryo-TEM images were used to calculate the mean number of iron oxide particles per liposomes, at least 200 liposomes were counted for each formulation. Values were compared using a Student's t-test, with a significance threshold of $p < 0.05$.

4.9. Inductively coupled plasma optical emission spectrometry

Inductively coupled plasma optical emission spectrometry (ICP-OES) was used for measuring the gadolinium (Gd), iron (Fe) and phosphorus (P) content of the liposome formulations. For that purpose, 10 μl of nitric acid were added to 100 μl of the liposome solutions and the samples were destructed at 80 °C overnight. Next, the samples were cooled down and introduced into the ICP-OES through a nebulizer. The intensities of this element-specific emission were used to determine the amount of Gd, Fe and P present in the samples. To calculate the mass quantities, the samples were compared to standardized solutions of Gd, Fe and P. All measurements were performed in triplicate.

4.10. MR data acquisition and analysis

All experiments were performed using a 1.5 T clinical whole-body MRI scanner (Philips Healthcare, Best, the Netherlands) equipped with a 8-channel head-coil for the *in vitro* sample characterizations and a small 47-mm circular coil for the kidney study.

4.10.1. Relaxation rate mapping

R_2 and R_2^* maps were acquired by using a multi spin-echo sequence (10 echoes, TR/TEfirst/ΔTE = 300/10/10 ms, NEX = 4, resolution = 0.6 × 0.6 × 2 mm^3 and a FOV = 72 x 72 mm, 6 slices, scan time = 15 min) and a multi-echo RF-spoiled gradient echo sequence (ME-SPGR , 16 echoes ,TR/TE_{first}/ΔTE = 120/4.61/4.61 ms, NEX = 4, resolution = 0.6 × 0.6 × 2 mm^3, matrix = 128 × 128, flip angle = 25°, 6 slices, scan time = 6 min), respectively. R_1 maps were measured using a Look-Locker acquisition (50) (resolution = 0.6 × 0.6 × 2 mm^3; FOV = 72 mm; TR = 4 s; α = 5°; images were acquired for 30 time points after the inversion, starting at 40 ms with 60 ms intervals, NEX = 2, 1 slice, scan time = 15 min). R_2 or R_2* were then determined on a voxel-by-voxel basis, by using a Levenberg-Marquardtfit of the functions [1] and [2] to the data, respectively:

$$S(TE) \propto S_0 e^{-TE \cdot R_2}, \tag{1}$$

$$S(TE,\ \Delta B_0/dz) \propto S_0 e^{-TE \cdot R_2^*} \cdot |\mathrm{sinc}(\gamma.(\Delta B_0/dz)/2.TE))|, \tag{2}$$

Here, S is the measured MR signal, S_0 is the signal when TE approaches 0, γ the gyromagnetic ratio and $\Delta B_0/dz$ the macroscopic main field inhomogeneity, more specifically the gradient in the slice direction, which was estimated based on the method previously described by Schaeffter *et al.* (51). Using the Look-Locker method (50), R_1 maps were calculated from the signal recovery after an inversion pulse:

$$S(t) \propto \left| A - Be^{-t(R_{1calc})} \right|, \tag{3}$$

where R_{1calc} is the relaxation time derived from a multiparametric fit to the signal intensity over time and α is the flip angle. The R_1 can then be estimated from R_{1calc} as:

$$R_{1real} = R_{1Calc} + \ln(\cos\alpha)/t \tag{4}$$

4.10.2. Relaxivity measurements

For each sample, the mean and standard deviation of R_1, R_2 and R_2^* were determined in a region-of-interest (ROI) of at least 30 voxels. The particles relaxivities were obtained from a linear regression of R_1, R_2 and R_2^* as a function of the phosphorus concentrations obtained from the ICP-OES measurements. All relaxivity estimations were performed at room temperature. All experiments were run in triplicate and the data is reported as mean ± SD. Calculations were done using custom scripts written in IDL (Exelis, Boulder, CO, USA).

4.11. Gd-TSM relaxivity change estimation

Assuming the Gd-TSM relaxation rate increased to be governed by the Gd release, measured Gd-TSM relaxivities variations were compared to relaxivity estimates obtained from the sum of r_{TSM} weighted by the iron concentration and $r_{Gd\text{-}TSL}$ weighted by the gadolinium concentration:

$$r_{Gd-TSM} = r_{Gd-TSL_m} \times \frac{[Gd]_{Gd-TSM}}{[P]_{Gd-TSM}} / \frac{[Gd]_{Gd-TSL}}{[P]_{Gd-TSL}} + r_{TSM_m} \times \frac{[Fe]_{Gd-TSM}}{[P]_{Gd-TSM}} / \frac{[Fe]_{TSM}}{[P]_{TSM}}, \tag{5}$$

4.12. Rabbit kidney experiments

4.12.1. Kidney resection

A total of five rabbit kidneys were collected from animals previously terminated in animal studies that were in compliance with the guidelines set by the institutional animal care committee and approved by the animal welfare committee of Utrecht University (Utrecht, the Netherlands). Prior to lethal injection by 4 mL of 200 mg.mL^{-1} pentobarbital, 2000 I.E. / rabbit of heparin was administered intravenously. Both the renal artery and the renal vein were clamped using a suture, as shown in Fig. 6a, keeping the

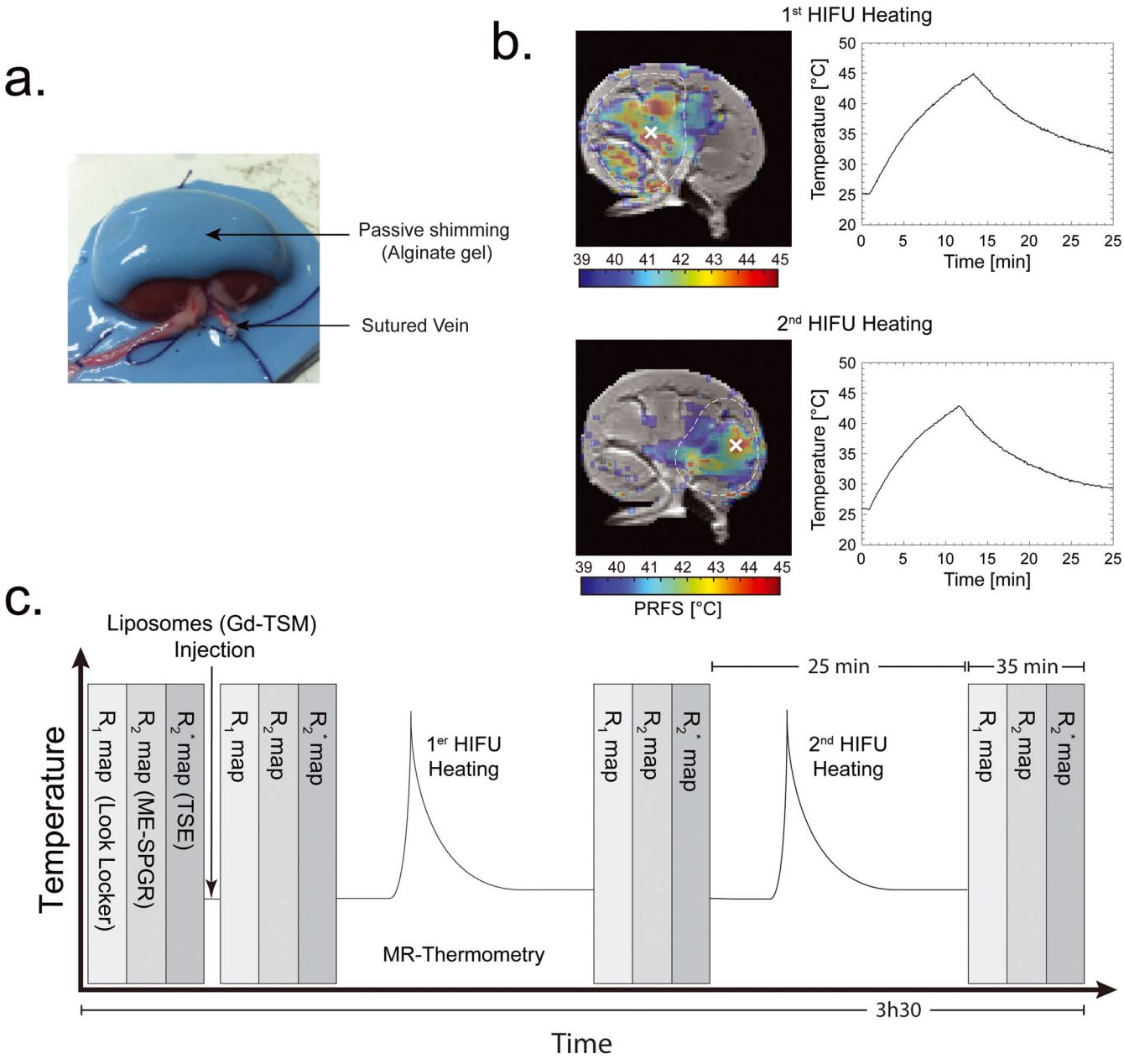

Figure 6. Kidney setup (a). T2 weighted magnitude images with thermometry map overlays measured on the basis of PRF-based thermometry, with the mean temperature profile over time measured in the displayed ROIs and the localization of the HIFU focal point (white cross) (b). Schematic of temporal MR scanning protocol (c).

vasculature system available for the liposome injection. Surrounding fatty tissues were removed from the kidneys. Right before the scanning session the kidney was included into an alginate impression gel (Cavex, Haarlem, the Netherlands), which served to limit the effect of air-tissue interfaces on R_2^*. All kidneys were used one to three days after the surgical resection. Three kidneys were injected with Gd-TSM and two control experiments were performed using the TSM and the Gd-TSL formulations, respectively.

4.12.2. *MR thermometry*

Proton resonance frequency shift (PRF)-based thermometry was calculated using the unwrapped phase change, $\Delta\Phi$, at the single echo time of a ME-SPGR dynamic sequence (TR/TE = 80/18.4 ms, flip angle = 25 °, NEX = 1, resolution = $1 \times 1 \times 3\,mm^3$ and a FOV = 62 x 62 mm, 1 slices, dynamic scan time = $4.97\,s.dyn^{-1}$, total scan time = 25 min). The temperature change ΔTn is related to $\Delta\Phi$ as follows: $\Delta T_n = \Delta\Phi/\beta \cdot \gamma \cdot TE \cdot B_0$ (52), with β being the temperature dependence of water chemical shift of -0.0101 ± 0.0004 ppm/°C (53). PRF-based thermometry was corrected for potential B_0 drift by using the phase of a reference agar gel (2% w/w $R_2^* \approx 20\,s^{-1}$), which was maintained at room temperature. The kidney setup with its corresponding PRF-based thermometry and the temporal MRI protocol are illustrated in Fig. 6b and Fig. 6c, respectively.

4.12.3. *HIFU exposure and MR imaging*

Ex vivo HIFU experiments were performed with an in-house-designed, spherical focused ultrasound transducer (Imasonic

SA, Besançon, France) integrated into the MRI table (54). The transducer had an operating frequency of 1.5 MHz and an acoustic pressure field centered at the focal point with a full width at half maximum of $1 \times 1 \times 6\,mm^3$. The HIFU sonications were performed with an acoustic power of 30 W during 15 min.

4.12.4. *Liposome injection and MR imaging*

After acquiring a first complete set of relaxation rate maps, 200 μL of Gd-TSM were injected in the vasculature system, prediluted 10 times to a concentration of 5.8 mM and 0.9 mM of gadolinium and iron, respectively. Then, two HIFU sonications located on the right and on the left of the kidney were successively performed and sets of relaxation maps were again acquired after the liposome injection and 15 min after each HIFU sonications. A schematic drawing of the setup is depicted in Fig. 6c.

Acknowledgements

Jeannette Smulders and Saskia Tromp-van den Bogaerdt (Philips Innovation Services - Material Analysis, Eindhoven, the Netherlands) are kindly acknowledged for the ICP-MS measurements of the liposome formulations. This work was supported by the Sound Pharma project (funded by the European Research Council, project number 268905 'Sound Pharma').

REFERENCES

1. Ferlay J, Steliarova-Foucher E, Lortet-Tieulent J, Rosso S, Coebergh JWW, Comber H, Forman D, Bray F. Cancer incidence and mortality patterns in Europe: Estimates for 40 countries in 2012. Eur J Cancer 2013; 49: 1374–1403. doi:10.1016/j.ejca.2012.12.027.
2. Gregoriadis G, Wills EJ, Swain CP, Tavill AS. Drug-carrier potential of liposomes in cancer chemotherapy. Lancet 1974; 1: 1313–1316.
3. Gabizon A, Catane R, Uziely B, Kaufman B, Safra T, Cohen R, Martin F, Huang A, Barenholz Y. Prolonged circulation time and enhanced accumulation in malignant exudates of doxorubicin encapsulated in polyethylene-glycol coated liposomes. Cancer Res 1994; 54: 987–992.
4. Gabizon AA. Pegylated Liposomal Doxorubicin: Metamorphosis of an Old Drug into a New Form of Chemotherapy. Cancer Invest 2001; 19: 424–436. doi:10.1081/CNV-100103136.
5. Immordino ML, Dosio F, Cattel L. Stealth liposomes: review of the basic science, rationale, and clinical applications, existing and potential. Int J Nanomedicine 2006; 1: 297–315.
6. Lasic DD. Novel applications of liposomes. Trends Biotechnol 1998; 16: 307–321. doi:10.1016/S0167-7799(98)01220-7.
7. Eloy JO, Claro de Souza M, Petrilli R, Barcellos JPA, Lee RJ, Marchetti JM. Liposomes as carriers of hydrophilic small molecule drugs: Strategies to enhance encapsulation and delivery. Colloids Surf B Biointerfaces 2014; 123: 345–363. doi:10.1016/j.colsurfb.2014.09.029.
8. Kwong B, Liu H, Irvine DJ. Induction of potent anti-tumor responses while eliminating systemic side effects via liposome-anchored combinatorial immunotherapy. Biomaterials 2011; 32: 5134–5147. doi:10.1016/j.biomaterials.2011.03.067.
9. Safra T, Muggia F, Jeffers S, Tsao-Wei DD, Groshen S, Lyass O, Henderson R, Berry G, Gabizon A. Pegylated liposomal doxorubicin (doxil): reduced clinical cardiotoxicity in patients reaching or exceeding cumulative doses of 500 mg/m2. Ann Oncol Off J Eur Soc Med Oncol ESMO 2000; 11: 1029–1033.
10. Koning GA, Eggermont AMM, Lindner LH, ten Hagen TLM. Hyperthermia and Thermosensitive Liposomes for Improved Delivery of Chemotherapeutic Drugs to Solid Tumors. Pharm Res 2010; 27: 1750–1754. doi:10.1007/s11095-010-0154-2.
11. Viglianti BL, Abraham SA, Michelich CR, Yarmolenko PS, MacFall JR, Bally MB, Dewhirst MW. In vivo monitoring of tissue pharmacokinetics of liposome/drug using MRI: Illustration of targeted delivery. Magn Reson Med 2004; 51: 1153–1162. doi:10.1002/mrm.20074.
12. Gaber MH, Wu NZ, Hong K, Huang SK, Dewhirst MW, Papahadjopoulos D. Thermosensitive liposomes: Extravasation and release of contents in tumor microvascular networks. Int J Radiat Oncol 1996; 36: 1177–1187. doi:10.1016/S0360-3016(96)00389-6.
13. Maruyama K, Unezaki S, Takahashi N, Iwatsuru M. Enhanced delivery of doxorubicin to tumor by long-circulating thermosensitive liposomes and local hyperthermia. Biochim Biophys Acta BBA - Biomembr 1993; 1149: 209–216. doi:10.1016/0005-2736(93)90203-C.
14. Li L, ten Hagen TLM, Bolkestein M, Gasselhuber A, Yatvin J, van Rhoon GC, Eggermont AMM, Haemmerich D, Koning GA. Improved intratumoral nanoparticle extravasation and penetration by mild hyperthermia. J Controlled Release 2013; 167: 130–137. doi:10.1016/j.jconrel.2013.01.026.
15. Kong G, Braun RD, Dewhirst MW. Characterization of the Effect of Hyperthermia on Nanoparticle Extravasation from Tumor Vasculature. Cancer Res 2001; 61: 3027–3032.
16. Kong G, Anyarambhatla G, Petros WP, Braun RD, Colvin OM, Needham D, Dewhirst MW. Efficacy of Liposomes and Hyperthermia in a Human Tumor Xenograft Model: Importance of Triggered Drug Release. Cancer Res 2000; 60: 6950–6957.
17. Manzoor AA, Lindner LH, Landon CD, Park J-Y, Simnick AJ, Dreher MR, Das S, Hanna G, Park W, Chilkoti A, Koning GA, ten Hagen TLM, Needham D, Dewhirst MW. Overcoming Limitations in Nanoparticle Drug Delivery: Triggered, Intravascular Release to Improve Drug Penetration into Tumors. Cancer Res 2012; 72: 5566–5575. doi:10.1158/0008-5472.CAN-12-1683.
18. Huang SK, Stauffer PR, Hong K, Guo JWH, Phillips TL, Huang A, Papahadjopoulos D. Liposomes and Hyperthermia in Mice: Increased Tumor Uptake and Therapeutic Efficacy of Doxorubicin in Sterically Stabilized Liposomes. Cancer Res 1994; 54: 2186–2191.
19. Viglianti BL, Ponce AM, Michelich CR, Yu D, Abraham SA, Sanders L, Yarmolenko PS, Schroeder T, MacFall JR, Barboriak DP, Colvin OM, Bally MB, Dewhirst MW. Chemodosimetry of in vivo tumor liposomal drug concentration using MRI. Magn Reson Med 2006; 56: 1011–1018. doi:10.1002/mrm.21032.
20. Lorenzato C, Cernicanu A, Meyre M-E, Germain M, Pottier A, Levy L, de Senneville BD, Bos C, Moonen C, Smirnov P. MRI contrast variation of thermosensitive magnetoliposomes triggered by focused ultrasound: a tool for image-guided local drug delivery. Contrast Media Mol Imaging 2013; 8: 185–192. doi:10.1002/cmmi.1515.
21. Ponce AM, Viglianti BL, Yu D, Yarmolenko PS, Michelich CR, Woo J, Bally MB, Dewhirst MW. Magnetic resonance imaging of temperature-sensitive liposome release: drug dose painting and antitumor effects. J Natl Cancer Inst 2007; 99: 53–63. doi:10.1093/jnci/djk005.
22. Tagami T, Foltz WD, Ernsting MJ, Lee CM, Tannock IF, May JP, Li S-D. MRI monitoring of intratumoral drug delivery and prediction of the therapeutic effect with a multifunctional thermosensitive liposome. Biomaterials 2011; 32: 6570–6578. doi:10.1016/j.biomaterials.2011.05.029.
23. de Smet M, Heijman E, Langereis S, Hijnen NM, Grüll H. Magnetic resonance imaging of high intensity focused ultrasound mediated drug delivery from temperature-sensitive liposomes: An in vivo proof-of-concept study. J Controlled Release 2011; 150: 102–110. doi:10.1016/j.jconrel.2010.10.036.
24. Staruch R, Chopra R, Hynynen K. Localised drug release using MRI-controlled focused ultrasound hyperthermia. Int J Hyperthermia 2011; 27: 156–171. doi:10.3109/02656736.2010.518198.
25. Ranjan A, Jacobs GC, Woods DL, Negussie AH, Partanen A, Yarmolenko PS, Gacchina CE, Sharma KV, Frenkel V, Wood BJ, Dreher MR. Image-guided drug delivery with magnetic resonance guided high intensity focused ultrasound and temperature sensitive liposomes in a rabbit Vx2 tumor model. J Controlled Release 2012; 158: 487–494. doi:10.1016/j.jconrel.2011.12.011.
26. Li L, ten Hagen TLM, Hossann M, Süss R, van Rhoon GC, Eggermont AMM, Haemmerich D, Koning GA. Mild hyperthermia triggered doxorubicin release from optimized stealth thermosensitive liposomes improves intratumoral drug delivery and efficacy. J Controlled Release 2013; 168: 142–150. doi:10.1016/j.jconrel.2013.03.011.
27. Partanen A, Yarmolenko PS, Viitala A, Appanaboyina S, Haemmerich D, Ranjan A, Jacobs G, Woods D, Enholm J, Wood BJ, Dreher MR. Mild hyperthermia with magnetic resonance-guided high-intensity focused ultrasound for applications in drug delivery. Int J Hyperthermia 2012; 28: 320–336. doi:10.3109/02656736.2012.680173.
28. Kruse DE, Lai C-Y, Stephens DN, Sutcliffe P, Paoli EE, Barnes SH, Ferrara KW. Spatial and Temporal-Controlled Tissue Heating on a Modified Clinical Ultrasound Scanner for Generating Mild Hyperthermia

in Tumors. IEEE Trans Biomed Eng 2010; 57: 155–166. doi:10.1109/TBME.2009.2029703.
29. Hijnen N, Langereis S, Grüll H. Magnetic resonance guided high-intensity focused ultrasound for image-guided temperature-induced drug delivery. Adv Drug Deliv Rev 2014; 72: 65–81. doi:10.1016/j.addr.2014.01.006.
30. Massart R. Preparation of aqueous magnetic liquids in alkaline and acidic media. IEEE Trans Magn 1981; 17: 1247–1248. doi:10.1109/TMAG.1981.1061188.
31. Laurent S, Forge D, Port M, Roch A, Robic C, Vander Elst L, Muller RN. Magnetic iron oxide nanoparticles: synthesis, stabilization, vectorization, physicochemical characterizations, and biological applications. Chem Rev 2008; 108: 2064–2110.
32. Wabler M, Zhu W, Hedayati M, Attaluri A, Zhou H, Mihalic J, Geyh A, DeWeese TL, Ivkov R, Artemov D. Magnetic resonance imaging contrast of iron oxide nanoparticles developed for hyperthermia is dominated by iron content. Int J Hyperthermia 2014; 30: 192–200. doi:10.3109/02656736.2014.913321.
33. Garnier B, Tan S, Miraux S, Bled E, Brisson AR. Optimized synthesis of 100 nm diameter magnetoliposomes with high content of maghemite particles and high MRI effect. Contrast Media Mol Imaging 2012; 7: 231–239. doi:10.1002/cmmi.487.
34. Ickenstein LM, Arfvidsson MC, Needham D, Mayer LD, Edwards K. Disc formation in cholesterol-free liposomes during phase transition. Biochim Biophys Acta BBA - Biomembr 2003; 1614(135–138). doi:10.1016/S0005-2736(03)00196-2.
35. Wu NZ, Klitzman B, Rosner G, Needham D, Dewhirst MW. Measurement of material extravasation in microvascular networks using fluorescence video-microscopy. Microvasc Res 1993; 46: 231–253. doi:10.1006/mvre.1993.1049.
36. Wu NZ, Da D, Rudoll TL, Needham D, Whorton AR, Dewhirst MW. Increased microvascular permeability contributes to preferential accumulation of Stealth liposomes in tumor tissue. Cancer Res 1993; 53: 3765–3770.
37. Hijnen NM, Elevelt A, Pikkemaat J, Bos C, Bartels LW, Grüll H. The magnetic susceptibility effect of gadolinium-based contrast agents on PRFS-based MR thermometry during thermal interventions. J Ther Ultrasound 2013; 1: 8. doi:10.1186/2050-5736-1-8.
38. Quesson B, de Zwart JA, Moonen CTW. Magnetic resonance temperature imaging for guidance of thermotherapy. J Magn Reson Imaging 2000; 12: 525–533. doi:10.1002/1522-2586(2000\10)12:4<525::AID-JMRI3>3.0.CO;2-V.
39. de Zwart JA, van Gelderen P, Kelly DJ, Moonen CT. Fast magnetic-resonance temperature imaging. J Magn Reson B 1996; 112: 86–90.
40. Xiao Y, Hong H, Javadi A, Engle JW, Xu W, Yang Y, Zhang Y, Barnhart TE, Cai W, Gong S. Multifunctional unimolecular micelles for cancer-targeted drug delivery and positron emission tomography imaging. Biomaterials 2012; 33: 3071–3082. doi:10.1016/j.biomaterials.2011.12.030.
41. Hong H, Zhang Y, Sun J, Cai W. Molecular imaging and therapy of cancer with radiolabeled nanoparticles. Nano Today 2009; 4: 399–413. doi:10.1016/j.nantod.2009.07.001.
42. Staruch RM, Ganguly M, Tannock IF, Hynynen K, Chopra R. Enhanced drug delivery in rabbit VX2 tumours using thermosensitive liposomes and MRI-controlled focused ultrasound hyperthermia. Int J Hyperthermia 2012; 28: 776–787. doi:10.3109/02656736.2012.736670.
43. Al-Jamal WT, Al-Ahmady ZS, Kostarelos K. Pharmacokinetics & tissue distribution of temperature-sensitive liposomal doxorubicin in tumor-bearing mice triggered with mild hyperthermia. Biomaterials 2012; 33: 4608–4617. doi:10.1016/j.biomaterials.2012.03.018.
44. Morita K, Zywietz F, Kakinuma K, Tanaka R, Katoh M. Efficacy of doxorubicin thermosensitive liposomes (40 °C) and local hyperthermia on rat rhabdomyosarcoma. Oncol Rep 2008; 20: 365–372. doi:10.3892/or_00000016.
45. Dicheva BM, Koning GA. Targeted thermosensitive liposomes: an attractive novel approach for increased drug delivery to solid tumors. Expert Opin Drug Deliv 2014; 11: 83–100. doi:10.1517/17425247.2014.866650.
46. Oude Blenke E, Mastrobattista E, Schiffelers RM. Strategies for triggered drug release from tumor targeted liposomes. Expert Opin Drug Deliv 2013; 10: 1399–1410. doi:10.1517/17425247.2013.805742.
47. Christian GD. Analytical Chemistry (6th edn). John Wiley & Sons: Hoboken, NJ, 2003.
48. Koning GA, Morselt HWM, Velinova MJ, Donga J, Gorter A, Allen TM, Zalipsky S, Kamps JAAM, Scherphof GL. Selective transfer of a lipophilic prodrug of 5-fluorodeoxyuridine from immunoliposomes to colon cancer cells. Biochim Biophys Acta BBA – Biomembr 1999; 1420: 153–167. doi:10.1016/S0005-2736(99)00091-7.
49. Oerlemans C, Deckers R, Storm G, Hennink WE, Nijsen JFW. Evidence for a new mechanism behind HIFU-triggered release from liposomes. J Controlled Release 2013; 168: 327–333. doi:10.1016/j.jconrel.2013.03.019.
50. Look DC, Locker DR. Time Saving in Measurement of NMR and EPR Relaxation Times. Rev Sci Instrum 1970; 41: 250–251. doi:10.1063/1.1684482.
51. Dahnke H, Schaeffter T. Limits of detection of SPIO at 3.0 T using T2* relaxometry. Magn Reson Med 2005; 53: 1202–1206. doi:10.1002/mrm.20435.
52. De Poorter J. Noninvasive MRI thermometry with the proton resonance frequency method: study of susceptibility effects. Magn Reson Med Off J Soc Magn Reson Med Soc Magn Reson Med 1995; 34: 359–367.
53. Peters RTD, Hinks RS, Henkelman RM. Ex vivo tissue-type independence in proton-resonance frequency shift MR thermometry. Magn Reson Med 1998; 40: 454–459. doi:10.1002/mrm.1910400316.
54. Haar GT, Coussios C. High intensity focused ultrasound: physical principles and devices. Int J Hyperth Off J Eur Soc Hyperthermic Oncol North Am Hyperth Group 2007; 23: 89–104.

SUPPORTING INFORMATION

Additional supporting information can be found in the online version of this article at the publisher's web site.